Fabrication and Evaluation Methods of Micro-structured Surfaces for Droplet Impact Experiments

Patrick Foltyn, Markus Guttmann, Marc Schneider, Stephanie Fest-Santini, Dorthe Wildenschild and Bernhard Weigand

Abstract The continuously increasing importance of micro-structured surfaces in technical applications and research require further development and use of reliable manufacturing processes as well as investigation methods for quality assurance. An overview of possible reproduction processes will be given and a new fabrication route in combination of laser lithography and nickel electroplating to provide stable mold inserts is introduced. Three methods for inspecting the reproduction quality of the polymeric micro-structured surfaces are presented discussing the respective advantages and disadvantages as well as the limiting factors diminishing the resolving power. The replication quality of four micro-structured surfaces produced with the hot embossing method is investigated, and the results are compared using these three techniques. Additionally, the principle investigation strategy of a test rig for droplet impact experiments on micro-structured surfaces is going to be outlined. Finally, preliminary results of droplet impacts on a structured surface are shown and discussed.

P. Foltyn (✉) · B. Weigand
Institute of Aerospace Thermodynamics (ITLR), University of Stuttgart,
Stuttgart, Germany
e-mail: patrick.foltyn@itlr.uni-stuttgart.de

M. Guttmann · M. Schneider
Institute of Microstructure Technology (IMT), Karlsruhe Institute of Technology,
Karlsruhe, Germany

S. Fest-Santini
Department of Management, Information and Production Engineering, University of Bergamo,
Dalmine (BG), Italy

D. Wildenschild
School of Chemical, Biological and Environmental Engineering, Oregon State University,
Corvallis, USA

1 Introduction

The research on micro-structured surfaces over the last 25 years has tremendously increased, as the number of annual publications is indicating. The statistics show the number of publications per year searching for "micro-structured surfaces" and "microstructured surfaces" in Google Scholar. While there were only 1320 items published in the year 2000, the number of publications in 2010 quintupled to 6950. In 2018, this number almost doubled again with 12670 publications. This strong increase shows significantly the growing importance of research with micro-structured surfaces. This can be explained by the scientific progress but also by the further increasing capabilities of manufacturing and investigation techniques as well as a technical need of such surfaces.

Based on the classical works of Wenzel in 1936 [28] as well as Cassie and Baxter in 1944 [2], many researchers have investigated the interaction of droplets with smooth and structured surfaces. Droplet impacts have been systematically investigated by Rioboo et al. [20] and Marengo et al. [13] using different surfaces with varying structure and wettability. Courbin et al. [3] have focused on the dynamics of the spreading and imbibition process on surfaces with well-defined micro-patterns. Especially complex surface structures are used to modify the surface wettability used for technical applications like self-cleaning surfaces or improved coating quality. An increase in surface roughness will lead to an increase of the intrinsic wettability in case of hydrophilic surfaces and to a decrease of the intrinsic wettability in case of hydrophobic surfaces [14]. For structured surfaces with a well-defined pattern, deposited droplets on these surfaces will deviate from spherical caps. As a consequence, a variation of the contact angle and the projected distance of the opposite triple points can be observed, as reported in [1, 3, 5, 12, 14]. A deviation of the outcomes compared to perfectly smooth surfaces can not be seen only for static droplet-structure interactions but also for dynamic droplet impacts on structured walls. One type of deviation is e.g. the determination of preferential wetting directions, [11, 22, 25]. In conclusion, the shape and the size of the structure pattern are main parameter on which the wetting morphology depends on significantly.

Consequently, a proper manufacturing and evaluation of these surfaces are very crucial for any research in this topic as well as for the technical applications. What follows, is an overview of possible manufacturing processes of which the mold insert fabrication for the hot embossing process is further outlined. Possible evaluation methods with the respective advantages and disadvantages and first experimental results for droplet impacts on structured surfaces are also discussed.

2 Surface Reproduction and Experimental Methods

2.1 Reproduction of Micro-structured Surface Samples

A vast number of different micro-fabrication techniques are available, which can be chosen in considering the used material, the dimensions of the structure, the number of reproductions and the application of the produced micro-structures. Among them are lithographic processes, etching processes, sputtering, additive micro-fabrications, micro-milling, or molding processes which can be used for the micro-fabrication [21]. For the evaluation of droplet impacts on micro-structured surfaces, it is advantageous to vary the structure patterns and the materials for different wetting behaviors. In the framework of the International Research Training Group "**Drop**let **I**nteraction **T**echnologies" (GRK 2160/1: DROPIT), an investigation of droplet impacts onto structured walls from the top and lateral perspective but also from the bottom view is envisaged. This requires not only a proper micro-structure but also a transparent material whenever possible. Therefore, the surface materials Lexan® (PC), Plexiglas® (PMMA) and Teflon® (PTFE) have been selected.

The produced patterns are steep grooves and arrays of steep squared pillars at micrometric dimensions, as they are depicted in Fig. 1 and given in Table 1. The grooves with a height of 20 µm are due to manufacturing requirements specifically very long pillars with a width of 60 µm and a length of 500 µm. In the direction of the grooves, a gap between each pillar of 15 µm can be found. The spacing perpendicular to the grooves is also 60 µm, see Fig. 1a. The squared pillars with an edge length of 60 µm, 30 µm or 15 µm have also a height of 20 µm, see Fig. 1b and Table 1. The spacing between each pillar is the same size as the width of the respective pillar. In conclusion, the solid fraction remains the same for all structures while the Wenzel roughness factor is increasing with decreasing edge length, see [2, 28]. Acquired images of the surfaces using three different techniques can be found in Figs. 3, 4 and 5.

The polymeric surface samples were manufactured by the Karlsruhe Nano Micro Facility (KNMF) at the Karlsruhe Institute of Technology (KIT), Germany, using
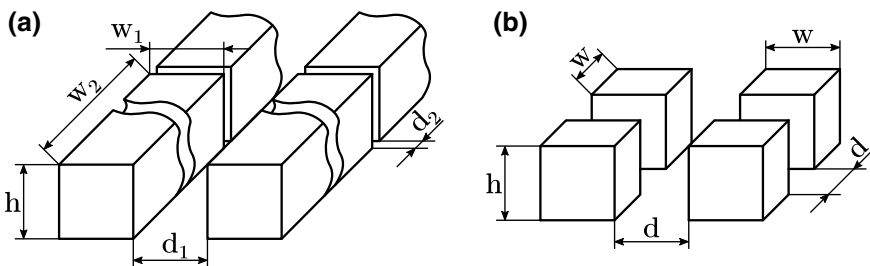
Fig. 1 Available structure patterns of **a** grooves and **b** pillars produced by the KNMF in Karlsruhe, Germany, with the given parameters in Table 1

Table 1 Dimensions of micro-structured surfaces. No. S1 corresponds to grooves, see Fig. 1a and no. S2-S4 are corresponding to pillars, see Fig. 1b

No.	Edge length	Distance	Height
S1	$w_1 = 60\,\mu m$, $w_2 = 500\,\mu m$	$d_1 = 60\,\mu m$, $d_2 = 15\,\mu m$	$h = 20\,\mu m$
S2	$w = 60\,\mu m$	$d = 60\,\mu m$	$h = 20\,\mu m$
S3	$w = 30\,\mu m$	$d = 30\,\mu m$	$h = 20\,\mu m$
S4	$w = 15\,\mu m$	$d = 15\,\mu m$	$h = 20\,\mu m$

**Table 2** Process parameters for the hot embossing reproduction of polymeric micro-structured surfaces

Material		Temperature		Force (kN)
		Embossing (°C)	Demolding (°C)	
Lexan®	(PC)	165	105	200
Plexiglas®	(PMMA)	140	40	200
Teflon®	(PTFE)	200	100	175

the hot embossing technique. This technique allows a high replication rate of micro-structured surfaces in pressing a mold with high pressure and temperature into the respective polymeric blank, see Table 2. A broad description of the hot embossing technique can be found e.g. in the book of Worgull [29]. Due to the high efforts of the mold insert production, all four structured patterns were placed next to each other with a blank area in between, see Fig. 2. After the production, the differently structured surfaces are cut into single pieces for the individual experiments.

2.2 Mold Insert Fabrication

The combination of laser lithography and electroplating was used to create a highly pressure and temperature stable thick nickel mold insert for hot embossing experiments. For the master fabrication, first, a 200 nm thick layer of antireflective coating *AZ BAR-Li* (*Microchemicals GmbH, Ulm Germany*), which is also an adhesion promotor, was spin-coated onto a 2 mm thick 4" silicon wafer and then baked at 200 °C for 60 s. Second, a 20 μm thick resist layer *MR10* (*micro resist technologies GmbH, Berlin, Germany*) was spin-coated, followed by a baking step at 95 °C for 30 min.

The latterly four described structure patterns were written into the photoresist with the laser writer *DWL66fs* (*Heidelberg Instruments GmbH, Heidelberg, Germany*) using a 10 mm write head at a laser power of 125 mW. The laser writing allows the fabrication of steep resist structures at micrometric dimensions, as they are depicted in Fig. 1 and given in Table 1. The written structures were then subjected to a Post Exposure Bake (PEB) at 75 °C and subsequently developed in PGMEA for 90 min.
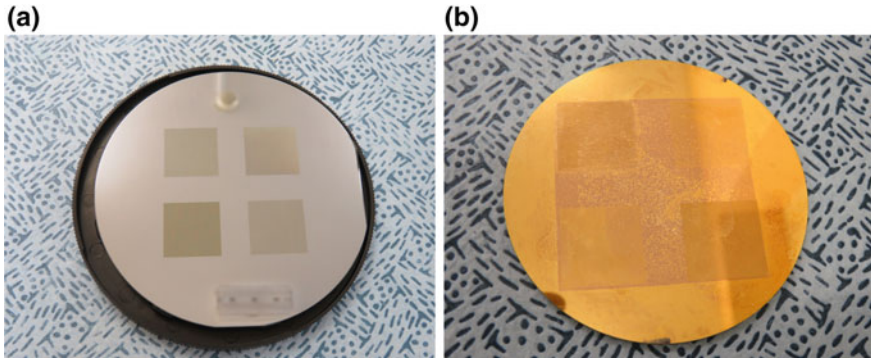
Fig. 2 **a** Silicon wafer with structured resist after laser lithography and **b** Nickel mold insert before removal of Cr/Au layer

A rinsing step in isopropanol and drying with air circulation at 30 °C terminates the fabrication of the structured master, see Fig. 2a. In order to transfer these polymeric structures into a stable metallic mold for the hot embossing process, thermal evaporation was used to prepare the resist structures for electroplating. 7 nm chromium acts as adhesive layer for a 50 nm gold layer as conducting plating base. Afterwards, a microscopic inspection of the resist structures was performed by means of SEM.

Nickel electroplating was carried out within a homemade boric acid containing nickel sulfamate electrolyte at a temperature of 52 °C (plating equipment with an electrolyte volume of 45 L from *Carl Dittmann GmbH & Co. KG, Karlsruhe, Germany*), a pH of 3.5 and a current density started at 0.1 A/dm^2 and increased up to 1.25 A/dm^2. To guarantee a good stability of the mold insert for the hot embossing experiments, the final thickness of the mold was chosen to 2.0 mm. To achieve this, galvanic deposition was carried out up to a height of approximately 2.8 mm (plating time ≈10 d). The desired height was realized using wire-EDM. To continue the mold fabrication, the thick silicon substrate was removed by wet-chemical etching with 30 w.−% KOH solution at 80 °C. The BAR-Li layer was removed by 15 min Reactive Ion Etching with O2 using *Etchlab 200–380 (Sentech GmbH, Berlin, Germany)* and the resist was stripped using O2/CF4 Plasma Etching (*STP2020; R3T GmbH, Taufkirchen, Germany*) for 30 min at 1200 W and 22 °C. To generate the final outer dimensions of the mold with a diameter of 81 mm, see Fig. 2b, the structures were protected by AZ resist and a second wire-EDM step was performed. After chemical treatment with *AZ400K (Microchemicals GmbH)* and isopropanol, followed by the wet-chemical etching of the Cr/Au metallization layers, the SEM characterization of the microstructures concludes the mold insert fabrication. The SEM showed, that all structural elements have been transferred in detail and with sharp edges, what can be also seen by the finally reproduced structure patterns in Figs. 3, 4 and 5.

2.3   Evaluation Methods for Investigating Micro-structured Surfaces

For evaluating micro-structured polymeric surfaces, a compromise between accuracy, effort and gathered information has to be found. In the following, three different methods for surface evaluation are presented: the classical optical microscopy, the Scanning Electron Microscopy (SEM) and the micro Computed Tomography (microCT). The mentioned methods were exemplarily carried out on the Lexan® surfaces.

The non-intrusive inspections of surface patterns for major damages using a classical optical microscope working with transmitted light is very fast, economical and easy. However, the two-dimensional perspective allows only the inspection in the direction of transmittance. This is the reason why local damages might not be detected properly because tilted sides or partial ruptures of the pillar bases might be hidden. Also the interpretation of the projected defects can be very difficult. However, globally extended or severe damages, like rip-off, missing pillars or not fully embossed structures can be detected.

The resolving power of light microscopes is limited to approximately $0.3\,\mu$m due to light diffraction and interference and can be calculated by the Abbe criterion:

$$d_0 = 0.61\lambda/(n \sin \alpha) \tag{1}$$

where d_0 represents the minimum resolvable separation, λ the wavelength of the light, n the refractive index and α the half-angle of the aperture of the microscope objective. The numerical aperture, defined as $n \sin \alpha$ is usually indicated on the respective microscope objectives. The calculated distance d_0 is the half diameter of the "Airy disk" which is the distance between the first-order peak and first-order trough of the focused light dot [27, 30].

A Scanning Electron Microscope (SEM) can be used if a higher magnification than approximately $1000\times$ of a classical optical microscope is needed. A well working electron optical system can create a beam diameter of 1 nm or finer, which will lead to a very high magnification. However, delocalization of imaging signals, constraints on beam size due to contrast and visibility considerations, mechanical stability of the setup and the vacuum, degradation of the sample and other influences can limit the resolving power. Nevertheless, for good experimental conditions a magnification of $100{,}000\times$ or more can be reached [8, 30]. SEM is also a non-intrusive method, if no sputtering of the samples is needed. Two advantages of SEM, which are helpful for the interpretation of structures, are a tiltable specimen stage, allowing also inspections of the structure from a non-perpendicular position, as well as a spatial view.

Both methods, the classical optical microscope and the SEM, are only two-dimensional imaging techniques. MicroCT, instead, is reconstructing a three-dimensional shape from single X-Ray projections, which have been acquired at several angle steps with help of reconstruction algorithms [18, 26]. The reconstructed geometries can be exported and used for further analysis e.g. in CAD-systems or for

numerical simulations. The resolving power of the microCT is dependent amongst other influences on the focal spot size of the X-Ray source, the number of projections, the pixel resolution of the X-Ray detector and the detector aperture [9]. Advanced microCT systems can achieve a resolving power of about 1 μm/voxel. For high resolving power, the sample needs to be small enough to allow optimal projection onto the detector, and must also be mounted very close to the X-Ray source. At a resolution of about 3–4 μm, the micro-structured surface samples had to be cut into 4×4 mm^2 sized pieces. Although the measurement principle itself is non-intrusive, this technique is intrusive for this application because of the need to cut samples down in size. Artifacts, e.g. due to non-optimal scan parameters (exposure time, energy levels, contrast challenges), a sample movement, degradation of the material by X-Rays and, if significant, X-Ray scattering can lead to lower reconstruction quality. Additionally, the low attenuation of thin polymeric structures can be a challenge for reconstruction.

2.4 Experimental Test Facility for Investigating Dynamic Droplet Impacts

The droplet impacts on micro-structured surfaces shall be investigated using three different perspectives. Two shadowgraphs, one from the top and one from the lateral perspective are captured simultaneously with one high-speed camera. This will help to determine the morphology of the droplet impact. The bottom view, captured by a second high-speed camera, is in a total-internal reflection configuration and allows to track the liquid spreading inside the structure and the imbibition into the structure. All three perspectives are acquired synchronously at 10 kHz and a resolution of 1 MPx. However, the results discussed in the following will be limited only to the lateral and the top view.

In future, the test rig shall be used to explore the occurring droplet impact phenomena on flat and structured surfaces for full-wetting cases but also for the complete range from wetting to non-wetting behavior.
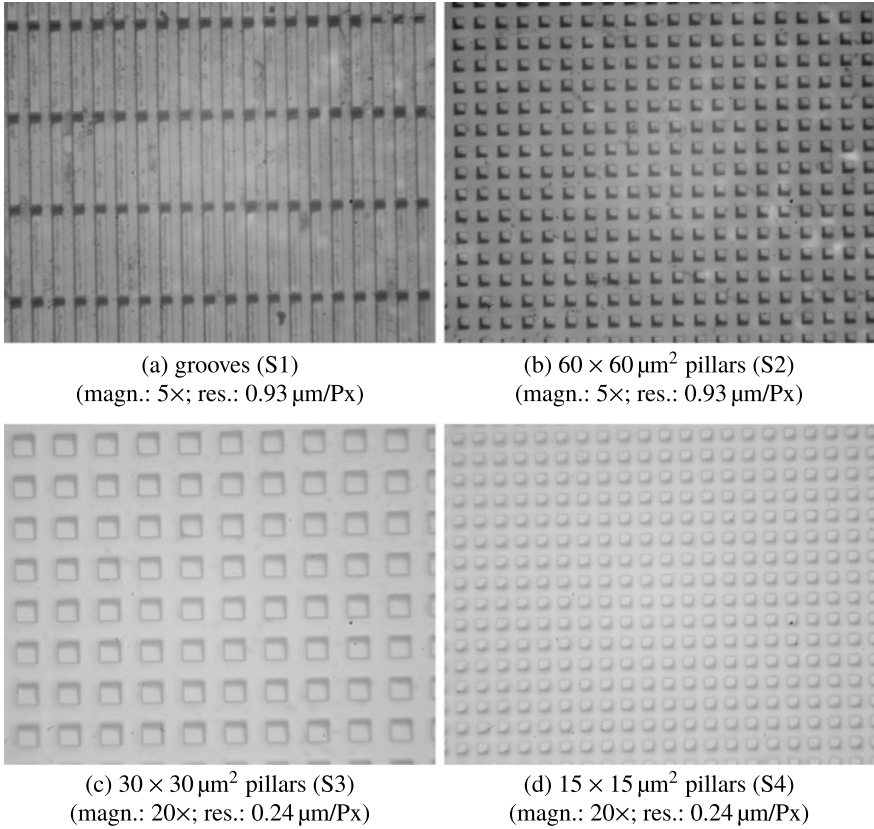
3 Results and Discussion

3.1 Surface Evaluation

The acquired images with the optical largefield microscope *LEITZ Metalloplan* are shown in Fig. 3. The resolution of the images is 0.93 μm/Px and 0.24 μm/Px, respectively. The increasing magnification was necessary due to an easier investigation of the finer structure items. One drawback of the optical microscope is the bad recognition of the topology of three-dimensional structures. Only by knowing

the structure beforehand, it can be determined which areas are elevated and which areas are the channels of the structure. For simple structures, like presented, this is "straight forward". For more complex structures, it can be helpful to adjust the focal plane incrementally in order to recognize the topology. This multifocal plane approach is also used by modern light microscopes rastering the focal planes and combining the images to one image with fully focal depth over the height of rastering. This avoids then blurriness for out of focus areas. Further, it is important to notice, that the images in Fig. 3, taken by an *IDS UI-3080CP-M-GL Rev.2* with 5.04 MPx and a resolution of 0.24 µm/Px is at the limit of the resolving power of the optical microscope. A further increase of pixels of the camera will not lead to a significant improvement of image quality due to the optical limitations as described in Sect. 2.3 and the Abbe criterion in Eq. (1). For a higher camera resolution, the not perfectly distinct structures will be only smeared over more pixels compared to cameras with a lower resolution.

The SEM images are displayed in Fig. 4. With the help of the significantly higher magnification, a spatial view and the tiltable specimen stage, some ridges on the top of the structure can be detected and measured. In the optical microscope, the corresponding areas of these ridges can be only detected by some darker areas on the structures, e.g. the top and right sides of each pillar in Fig. 3c. Though, the proper interpretation of these areas would have been almost impossible without the SEM investigations. The output of the SEM are only two-dimensional pictures, as shown in Fig. 4. For measuring the dimension of the ridges or also the whole pillars, it is only possible to obtain the dimensions such as the height or the depth in considering the projection of the tilted structure onto the image plane. The tilt of the specimen stage for the shown images is set to 30°.

In contrast to this, the reconstructed microCT-scans, with a resolution of 3.3 µm/voxel in Fig. 5, can give much more information about the pillar shape. With the help of a specially developed routine for evaluating the ridge height, the shape of the pillars and height of the ridges can be determined, see also Fig. 6. However, in comparison to the SEM and the optical microscope, the resolving power of the microCT is usually significantly lower in part because of the very low X-Ray attenuation of the material. This means that features, which are in the size of two voxels and smaller, might not be resolved properly. But also for larger features, the resolving power might not be sufficiently high. The smallest pillars with an edge length of 15 µm (surface S4) are only represented by approximately 5 voxel for each spatial direction. This leads to a blurry and not well defined shape, so that often no orthogonal edges can be determined, see Fig. 5d. The challenge in the post-processing of reconstructed microCT-data is to transform the voxelized representation of surfaces into a smooth triangulated surface. This will make the surfaces usable for further investigations such as numerical simulations. There are several smoothing routines in commercial software packages like *Avizo* [24], but also in open-source software. For this post-processing step, a compromise between smoothing and shape conservation has to be found. In conclusion, a change of shape due to smoothing is acceptable if its magnitude is far lower than the resolution of the microCT scans. Under consideration of the limits in resolving power and the need of smoothing, the possibility
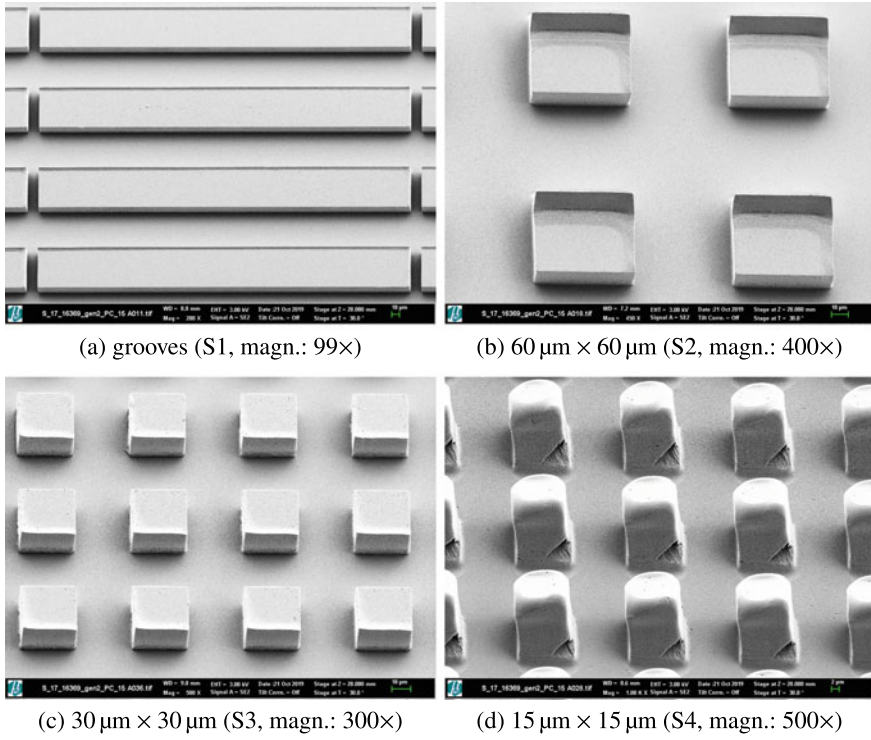
(a) grooves (S1)
(magn.: 5×; res.: 0.93 μm/Px)

(b) 60 × 60 μm² pillars (S2)
(magn.: 5×; res.: 0.93 μm/Px)

(c) 30 × 30 μm² pillars (S3)
(magn.: 20×; res.: 0.24 μm/Px)

(d) 15 × 15 μm² pillars (S4)
(magn.: 20×; res.: 0.24 μm/Px)

Fig. 3 Micro-structured Lexan®-surfaces of different dimensions acquired with optical microscope using a combination of transmitted and reflected light. The magnification of each image is given at the respective image

of the surface export is, nevertheless, very powerful, since simulations can use the same surface patterns for droplet impacts as the experiment itself. The magnitude of deviations between real, exported surfaces and perfect, generic surfaces on the outcome of numerical simulations of droplet impacts will be investigated in the future. Here, also the influence of resolving power of the microCT on the numerical results need to be studied.

In the following, the dimension of one single but "defect" 60 μm pillar of the reconstructed microCT S2 surfaces is analyzed. For the detailed analysis, a separate microCT-scan was performed with a resolution of 2.7 μm/voxel and compared to SEM images. Due to sample preparation and availability of the measurement devices, the scanned surface samples were not identical so that not exactly the same pillar was measured with the SEM and microCT. The surface was reconstructed, exported and the profile along several slices of the pillar analyzed, as depicted in Fig. 6. The

(a) grooves (S1, magn.: 99×)   (b) 60 μm × 60 μm (S2, magn.: 400×)

(c) 30 μm × 30 μm (S3, magn.: 300×)   (d) 15 μm × 15 μm (S4, magn.: 500×)

Fig. 4 Micro-structured Lexan®-surfaces of different dimensions acquired with Scanning Electron Microscopy (SEM). The magnification of each image is given at the respective image. The specimen stage was tilted by 30°

elevation of the ridge measured by microCT was about 3 voxel or approximately 8 μm and matches very well to the SEM measurements. These findings were expected, since the production procedure can be considered as very reliable during the hot embossing process. The reason for the partially elevated rim might be a sticking nickel mold on the pillars side during the demolding phase of the hot embossing process. The resulting high local forces lead to the observed local deformations in case of large pillars or might elongate the whole pillar in case of smaller edge lengths. In general, the influence of non-perfectly shaped pillars are assumed to be neglectable since the magnitude as well as the number of defect pillars are not very high. However, a numerical simulation of droplets impacting on these exported surfaces might give further information in the future.

(a) grooves (S1)	(b) 60 μm × 60 μm pillars (S2)
(c) 30 μm × 30 μm pillars (S3)	(d) 15 μm × 15 μm pillars (S4)
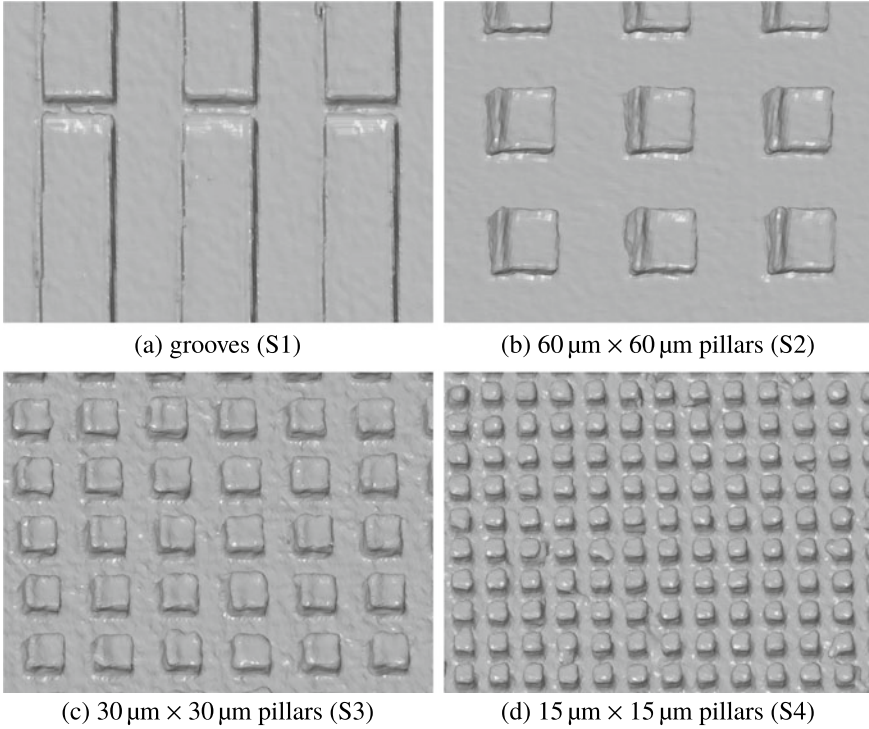
Fig. 5 Micro-structured Lexan®-surfaces of different dimensions acquired with micro Computed Tomography (microCT), reconstructed and exported as stl.-surface. Resolution: 3.3 μm/voxel

3.2 Droplet Impact on Micro-structured Surfaces

Preliminary experiments on the previously mentioned test rig are used to determine the fundamental morphology of droplet impacts on such micro-structured surfaces. For the experiment presented in the following a blunt needle with 0.40 mm outer and 0.22 mm inner diameter was used as droplet generator. The produced droplets had always a reproducible diameter D in the range of (1.78 ± 0.03) mm and a reproducible velocity u_{imp} in the range of (1.22 ± 0.01) m/s. The Reynolds number Re, Weber number We, Capillary number Ca and Ohnesorge number Oh can be calculated as follows [19]:

$$Re = \frac{\rho D u_{\mathrm{imp}}}{\mu}, \qquad We = \frac{\rho D u_{\mathrm{imp}}^2}{\sigma}, \qquad Ca = \frac{u_{\mathrm{imp}}\mu}{\sigma}, \qquad Oh = \frac{\mu}{\sqrt{\rho D \sigma}} \qquad (2)$$
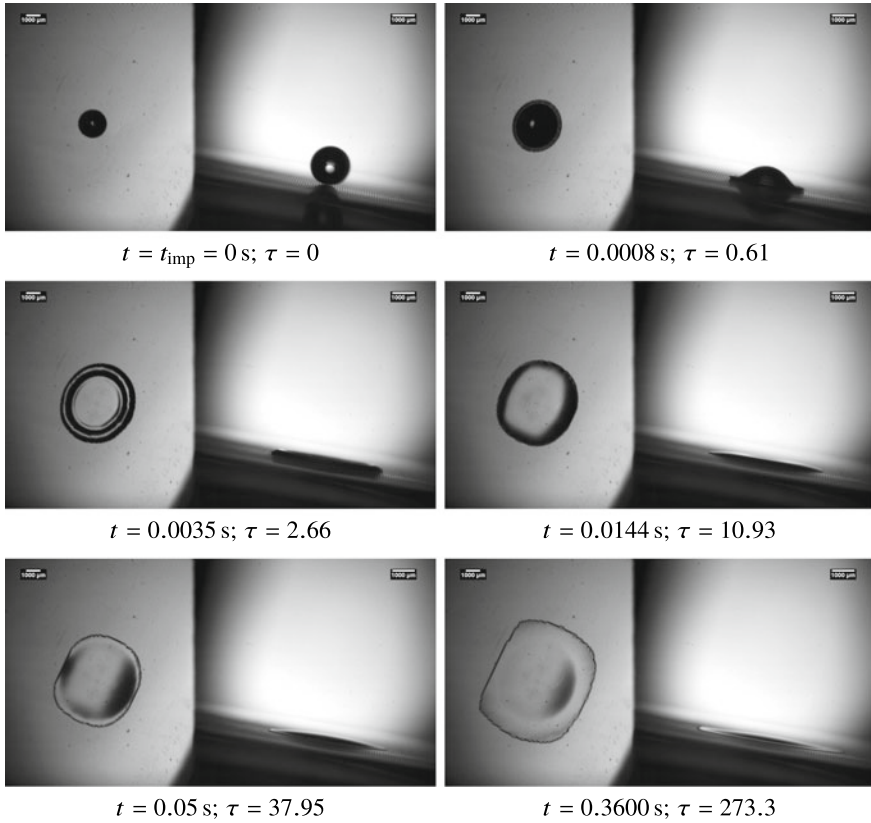
The dimensionless time τ for the droplet impact is defined as

$$\tau = t \frac{u_{\text{imp}}}{D} \tag{3}$$

In the following, a droplet impact of isopropanol (2-propanol) with a diameter of $D = 1.77$ mm and an impact velocity of $u_{\text{imp}} = 1.22$ m/s will be further discussed, see also Fig. 7. The density for isopropanol, the surface tension and the dynamic viscosity of $\rho = 785$ kg/m^3, $\sigma = 23.0$ mN/m and $\mu = 2.43$ mPa s have been used [15, 23]. With Eqs. (2) the dimensionless parameters can be determined to: $Re = 699.3$, $We = 90.5$, $Ca = 0.129$ and $Oh = 0.0136$. The free surface energies for isopropanol, $\sigma_L^p = 3.5$ mN/m and $\sigma_L^d = 19.5$ mN/m, [15], can predict a full-wetting behavior on flat PC surfaces using the OWRK-model [10, 16, 17]. Consequently, it can be expected that for all kind of structures on the PC-wafer a full-wetting behavior will occur. This can be confirmed by the experiments on $60 \times 60 \, \mu\text{m}^2$ pillars of PC (surface S2).
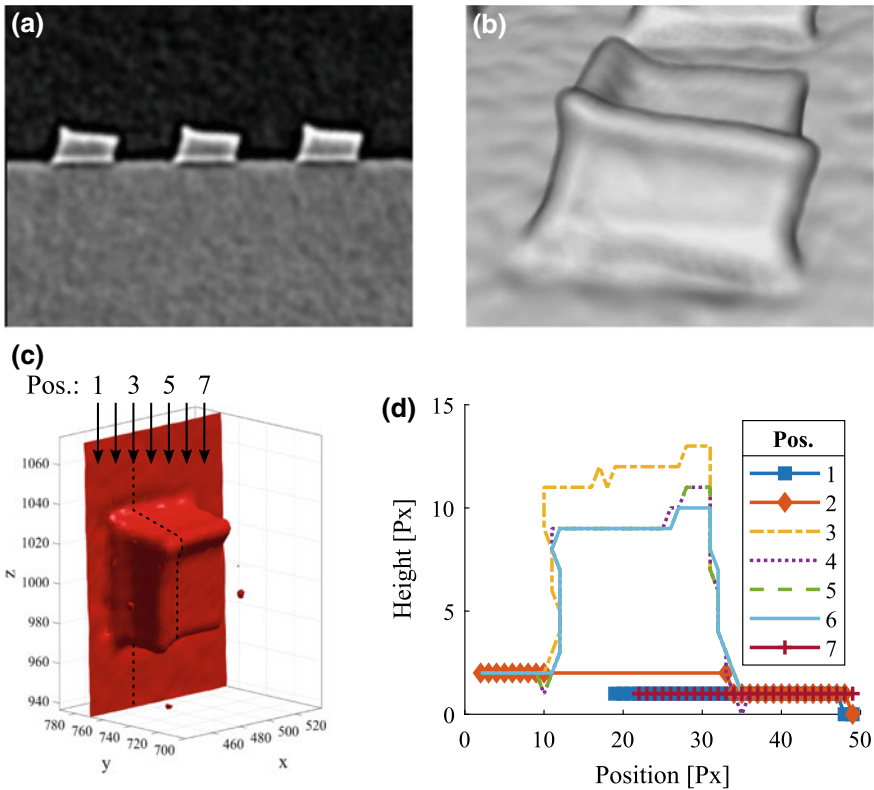
Fig. 6 Procedure for the evaluation of one single pillar with an edge length of 60 μm (surface S2) acquired by microCT with 2.7 μm/voxel: **a** single slice of reconstructed three-dimensional volume, **b** volume rendering of reconstructed three-dimensional volume, **c** exported single pillar with positions of sections, **d** height profile of each slice

$t = t_{\text{imp}} = 0\,\text{s};\ \tau = 0$ $t = 0.0008\,\text{s};\ \tau = 0.61$

$t = 0.0035\,\text{s};\ \tau = 2.66$ $t = 0.0144\,\text{s};\ \tau = 10.93$

$t = 0.05\,\text{s};\ \tau = 37.95$ $t = 0.3600\,\text{s};\ \tau = 273.3$

Fig. 7 Chronological sequence of a drop impact of isopropanol with a diameter of $D = 1.77\,\text{mm}$ and an impact velocity of $u_{\text{imp}} = 1.22\,\text{m/s}$ on a structured PC surface (S2) with $60 \times 60\,\mu\text{m}^2$ pillars at a $Re = 699.3$ and $We = 90.5$. Left image: top view, scale: $29.8\,\mu\text{m/pixel}$; right image: lateral view, scale: $19.2\,\mu\text{m/pixel}$

The overall morphology is following a deposition behavior and match the described splash/non-splash limits in [19], see Fig. 7. Two spreading regimes can be observed, the inertia driven spreading at the beginning of the droplet impact and the viscous spreading during the end of the impact. The inertia driven regime occurs at $\tau \lesssim 10.93$. The very slow spreading viscous regime at $\tau \gtrsim 10.93$ is mainly driven by capillary forces and follows the observations of [4]. The authors have observed a "zipping" of the liquid, which is the energetically favorable way of viscous imbibition into micro-structures. If one row of pillars is completely filled with liquid, the liquid will advance at a very limited area, mostly in between two pillars, to the next row. Afterwards, the liquid is "zipping" to the side filling the whole row inside the structure until the liquid will proceed to the next row of pillars.

3.3 Film Thickness Measurement of Droplet Lamella

During the droplet impact on smooth surfaces, the formation of a droplet lamella can be expected. Thickness measurements of droplet lamellas are very challenging due to the high dynamics of the impact and the large range of expected film thicknesses. The experimental test rig, will use the newly developed LASER Pattern Shift Method (LPSM) to measure the lamella thickness during the droplet impact. The method is evaluating the parallel shift of a laser pattern which is directly proportional to the film height, [6]. In using the Position Sensitive Detector (PSD) *1L30_SU2* of *SITEK Electro Optics*, the sampling rate can be increased to 500 kHz so that the temporal development of the lamella thickness can be captured [7].

The development of the LPSM will be continued, in order to measure the liquid film thickness inside the structure during the droplet impact. A three-dimensional profile of the film thickness as output will then give further information about the liquid distribution which can be used e.g. for validating detailed numerical simulations.

4 Conclusion

The influence of micro-structures on deposited droplets and droplet impacts can be determined by deviations from the spherical shape and preferential spreading directions. The dimensions of structure have a significant influence of the outcome. Therefore, a high reproduction quality and reliable inspection technique for such micro-structured surfaces are needed. Due to the requirements of dimensions and shape, the surfaces were produced with the hot embossing process. Also other reproduction possibilities for micro-structured surfaces were mentioned. As investigation methods for the surface structure the optical largefield microscope, the Scanning Electron Microscopy (SEM) and the micro Computed Tomography (microCT) have been used. While the Abbe criterion is mainly limiting the resolving power of the optical microscope the quality of SEM is limited by the electron beam quality. The resolving power of microCT is mainly influenced by focal spot size and the specimen size, and limited by X-Ray absorption, which is what produces image contrast. Choosing the right method is not easy, since it is always a compromise between availability of the technique, effort and information which can be extracted from the different techniques. The optical largefield microscope and SEM are two imaging methods, which can be used for measuring the dimensions from the images. However, the projection into the image plane needs to be considered for the determination of dimensions. Both techniques are either very economical or can provide a very high magnification of up to 100,000× or more. MicroCT, instead, has a lower resolving power, but can provide an export of the digitalized volumes of the scanned surfaces. These exported volumes can be then used e.g. for numerical simulations. The analyzed micro-structured surfaces show mainly a proper reproduction quality.

The influence of the deviation between experimental and generic surfaces onto the droplet impact outcomes needs to be numerically investigated in the future. Finally, preliminary results of a droplet impact on the structured surfaces have shown preferential spreading directions. Future investigations will then also focus on the effect of the flow inside the structure and on the heat transfer on micro-structured walls.

References

1. Bico, J., Tordeux, C., Quéré, D.: Rough wetting. Europhysics Letters (EPL) **55**(2), 214–220 (2001). https://doi.org/10.1209/epl/i2001-00402-x
2. Cassie, A.B.D., Baxter, S.: Wettability of porous surfaces. Trans. Faraday Soc. **40**, 546–551 (1944). https://doi.org/10.1039/TF9444000546
3. Courbin, L., Bird, J.C., Reyssat, M., Stone, H.A.: Dynamics of wetting: from inertial spreading to viscous imbibition. J. Phys.: Condens. Matter **21**(46), 464127 (2009). http://stacks.iop.org/0953-8984/21/i=46/a=464127
4. Courbin, L., Denieul, E., Dressaire, E., Roper, M., Ajdari, A., Stone, H.A.: Imbibition by polygonal spreading on microdecorated surfaces. Nat. Mater. **6**(9), 661–664 (2007). https://doi.org/10.1038/nmat1978
5. Foltyn, P., Restle, F., Weigand, B.: 360° evaluation of projected contact angles of static droplets on structured surfaces. In: Droplet Impact Phenomena & Spray Investigations (DIPSI), Bergamo, Italy (2019). https://doi.org/10.6092/DIPSI2019
6. Foltyn, P., Roth, N., Weigand, B.: Development and calibration of the laser pattern shift method for measuring the lamella topology during drop impact on walls. In: 29th European Conference on Liquid Atomization and Spray Systems, Paris, France (2019)
7. Foltyn, P., Roth, N., Weigand, B.: Verfahren zur Messung der Schichtdicke einer optisch transparenten Schicht, insbesondere einer Flüssigkeitsschicht. EP 19 192 074.3 application (2019)
8. Goldstein, J.I.V., Joy, D.C., Michael, J.R., Ritchie, N.W., Scott, J.H.J. (eds.): Scanning Electron Microscopy and X-Ray Microanalysis, 4th ed. 2018 edn. SpringerLink. Bücher. Springer, New York, NY (2018). https://doi.org/10.1007/978-1-4615-0215-9. Online-Ressource (XXIII, 550 p. 546 illus., 409 illus. in color, online resource)
9. Hsieh, J.V. (ed.): Computed Tomography: Principles, Design, Artifacts, and Recent Advances, 3rd ed. edn. SPIE Press monograph ; PM259. SPIE Press, Bellingham, Wash (2015). http://dx.doi.org/10.1117/3.2197756. Online-Ressource
10. Kaelble, D.H.: Dispersion-polar surface tension properties of organic solids. J. Adhes. **2**(2), 66–81 (1970). https://doi.org/10.1080/0021846708544582
11. Kim, S.J., Kim, J., Moon, M.W., Lee, K.R., Kim, H.Y.: Experimental study of drop spreading on textured superhydrophilic surfaces. Phys. Fluids **25**(9), 092110 (2013). https://doi.org/10.1063/1.4821985
12. Kim, D., Pugno, N.M., Ryu, S.: Wetting theory for small droplets on textured solid surfaces. Sci. Rep. **6**, 37813 (2016). https://doi.org/10.1038/srep37813

13. Marengo, M., Antonini, C., Roisman, I.V., Tropea, C.: Drop collisions with simple and complex surfaces. Curr. Opin. Colloid & Interface Sci. **16**(4), 292–302 (2011). https://doi.org/10.1016/j.cocis.2011.06.009. http://www.sciencedirect.com/science/article/pii/S1359029411000859

14. McHale, G., Shirtcliffe, N.J., Aqil, S., Perry, C.C., Newton, M.I.: Topography driven spreading. Phys. Rev. Lett. **93**, 036102 (2004). https://doi.org/10.1103/PhysRevLett.93.036102

15. Ohm, A., Lippold, B.: Charakterisierung der benetzbarkeit von arzneistoffpulvern mit hilfe der sessile-drop technik, teil 2: Kritische oberflächenspannung und randwinkel/oberflächenspannungskurven. Pharm. Ind. **48**(5), 508–513 (1986)

16. Owens, D.K., Wendt, R.C.: Estimation of the surface free energy of polymers. J. Appl. Polym. Sci. **13**(8), 1741–1747 (1969). https://doi.org/10.1002/app.1969.070130815

17. Rabel, W.: Einige Aspekte der Benetzungstheorie und ihre Anwendung auf die Untersuchung und Veränderung der Oberflächeneigenschaften von Polymeren. Farbe und Lacke **77**(10), 997–1005 (1971)

18. Radon, J.: über die bestimmung von funktionen durch ihre integralwerte längs gewisser mannigfaltigkeiten. In: Berichte über die Verhandlungen der Königlich-Sächsischen Akademie der Wissenschaften zu Leipzig, Mathematisch-Physische Klasse, vol. 69, pp. 262–277. Teubner, Leipzig (1917)

19. Rein, M., Delplanque, J.P.: The role of air entrainment on the outcome of drop impact on a solid surface. Acta Mechanica **201**(1), 105 (2008). https://doi.org/10.1007/s00707-008-0076-9

20. Rioboo, R., Tropea, C., Marengo, M.: Outcomes from a drop impact on solid surfaces. Atomization and Sprays **11**(2), (2001)

21. Silverio, V., Cardoso de Freitas, S.: Microfabrication techniques for microfluidic devices, Chap. 2, pp. 25–51. Springer International Publishing, Cham (2018). https://doi.org/10.1007/978-3-319-59593-1_2

22. Stapelbroek, B.B.J., Jansen, H.P., Kooij, E.S., Snoeijer, J.H., Eddi, A.: Universal spreading of water drops on complex surfaces. Soft Matter **10**, 2641–2648 (2014). https://doi.org/10.1039/C3SM52464G

23. Th.Geyer: Safety data sheet according to 1907/2006/ec, article 31. Tech. rep., Th. Geyer GmbH & Co. KG (2017). https://shop.thgeyer-lab.com/erp/zertifikate/searchSDB_or_COA.action?artikel=11646872&isDirectLink=true&searchSDB=true&hersteller=740

24. Thermo Fisher Scientific: User's Guide Avizo Software 2019 (2019). https://assets.thermofisher.com/TFS-Assets/MSD/Product-Guides/users-guide-avizo-software-2019.pdf

25. Vaikuntanathan, V., Sivakumar, D.: Maximum spreading of liquid drops impacting on groove-textured surfaces: Effect of surface texture. Langmuir **32**(10), 2399–2409 (2016). https://doi.org/10.1021/acs.langmuir.5b04639. PMID: 26885767

26. van Aarle, W., Palenstijn, W.J., Beenhouwer, J.D., Altantzis, T., Bals, S., Batenburg, K.J., Sijbers, J.: The astra toolbox: a platform for advanced algorithm development in electron tomography. Ultramicroscopy **157**, 35–47 (2015). https://doi.org/10.1016/j.ultramic.2015.05.002. http://www.sciencedirect.com/science/article/pii/S0304399115001060

27. Watt, I.M.V. (ed.): The Principles and Practice of Electron Microscopy, 2nd edn. Cambridge University Press, Cambridge [U.A.] (1997)

28. Wenzel, R.N.: Resistance of solid surfaces to wetting by water. Ind. Eng. Chem. **28**(8), 988–994 (1936). https://doi.org/10.1021/ie50320a024

29. Worgull, M.: Hot Embossing: Theory and Technology of Microreplication (Micro and Nano Technologies). Elsevier (2009). https://www.sciencedirect.com/book/9780815515791/hot-embossing

30. Zhou, W., Apkarian, R., Wang, Z.L., Joy, D.: Fundamentals of Scanning Electron Microscopy (SEM), pp. 1–40. Springer New York, New York, NY (2007). https://doi.org/10.1007/978-0-387-39620-0_1